LETTER

doi:10.1038/nature12801

Dissipative production of a maximally entangled steady state of two quantum bits

Y. Lin[1]*, J. P. Gaebler[1]*, F. Reiter[2], T. R. Tan[1], R. Bowler[1], A. S. Sørensen[2], D. Leibfried[1] & D. J. Wineland[1]

Entangled states are a key resource in fundamental quantum physics, quantum cryptography and quantum computation[1]. Introduction of controlled unitary processes—quantum gates—to a quantum system has so far been the most widely used method to create entanglement deterministically[2]. These processes require high-fidelity state preparation and minimization of the decoherence that inevitably arises from coupling between the system and the environment, and imperfect control of the system parameters. Here we combine unitary processes with engineered dissipation to deterministically produce and stabilize an approximate Bell state of two trapped-ion quantum bits (qubits), independent of their initial states. Compared with previous studies that involved dissipative entanglement of atomic ensembles[3] or the application of sequences of multiple time-dependent gates to trapped ions[4], we implement our combined process using trapped-ion qubits in a continuous time-independent fashion (analogous to optical pumping of atomic states). By continuously driving the system towards the steady state, entanglement is stabilized even in the presence of experimental noise and decoherence. Our demonstration of an entangled steady state of two qubits represents a step towards dissipative state engineering, dissipative quantum computation and dissipative phase transitions[5–7]. Following this approach, engineered coupling to the environment may be applied to a broad range of experimental systems to achieve desired quantum dynamics or steady states. Indeed, concurrently with this work, an entangled steady state of two superconducting qubits was demonstrated using dissipation[8].

Trapped ions are one of the leading experimental platforms for quantum information processing, and advanced protocols using unitary quantum gates have been demonstrated (see, for example, refs 9, 10). However, decoherence and dissipation from coupling to the environment remains a challenge. One approach to overcome this relies on active feedback[11–17]. Such feedback techniques may be extended to quantum error correction, which can stabilize entangled states or realize fault-tolerant quantum computations. This will, however, require high-fidelity quantum gates and large qubit overheads that are beyond the reach of current experiments[2]. Recently, a complementary approach has been proposed to create entangled states or perform quantum computing by engineering the continuous interaction of the system with its environment[5–7,18–28]. In our experiment, we take a step towards harnessing dissipation for quantum information processing by producing an entangled state that is inherently stabilized against decoherence by the applied interactions in a setting fully compatible with quantum computation. With this technique, we realize maximally entangled steady states with a fidelity of $F = 0.75(3)$ by simultaneously applying a combination of time-independent fields. We also demonstrate that a stepwise application of these fields can speed up the dynamics of the scheme and achieve a fidelity of $F = 0.89(2)$ after approximately 30 repetitions. In both cases, the errors can be attributed to known experimental imperfections. Although these errors lead to a lower fidelity for entanglement preparation in our system as compared to unitary gates[10], the dissipative technique is much less sensitive to certain sources of experimental noise—for example, laser intensity fluctuations common to both qubits—and so may lead to improved performance in other trapped-ion systems where this is the dominant error. In the Supplementary Information we model the errors for the dissipative entanglement preparation and propose how they can be reduced.

Our scheme uses an ion chain with two qubit ions and at least one 'coolant' ion for sympathetic cooling[29] of the qubit ions' motion. We consider a normal motional mode of this ion chain having frequency ν and mean motional quanta $\bar{n}$. We cool the motional mode to $\bar{n} \approx 0$ by laser-cooling the coolant ion (or ions) and thus effectively couple the vibration to a zero-temperature bath with the phonon loss rate denoted by κ. As depicted in Fig. 1, we consider four energy levels of each qubit ion ($^9Be^+$), where $|\uparrow\rangle$ and $|\downarrow\rangle$ are the qubit 'spin' states, $|a\rangle$ is an auxiliary state and $|e\rangle$ is a fast-decaying excited electronic state. A sideband excitation, with Hamiltonian $H_s \equiv \Omega_s(|\uparrow\rangle_1\langle\downarrow| + |\uparrow\rangle_2\langle\downarrow|)b^+ + \text{h.c.}$ in the atomic and motional rotating frame, couples the two ions' spins via their motion (here Ω_s denotes the Rabi frequency, b^+ is the motional-mode Fock-state creation operator, the number subscripts denote the qubit ion number, and h.c. is the Hermitian conjugate). A carrier interaction with Hamiltonian $H_c \equiv \Omega_c(|a\rangle_1\langle\uparrow| + |a\rangle_2\langle\uparrow|) + \text{h.c.}$ drives the $|\uparrow\rangle \leftrightarrow |a\rangle$ transition of each ion with Rabi frequency Ω_c, and a repump laser incoherently drives $|a\rangle \rightarrow |\downarrow\rangle$, $|\uparrow\rangle$ by coupling to the intermediate state $|e\rangle$ at a rate γ (see Fig. 1a). All the above transitions are homogeneously driven for both qubit ions, such that individual addressing is not needed for this scheme. These couplings ensure that the maximally entangled singlet state $|S\rangle \equiv \frac{1}{\sqrt{2}}(|\uparrow\downarrow\rangle - |\downarrow\uparrow\rangle)$ is the only steady state of the effective dynamics[30] in the regime $\gamma, \kappa, \Omega_c \ll \Omega_s$.

For an intuitive understanding of the scheme, we first consider only the sideband excitation and the sympathetic cooling (blue lines in Fig. 1a), which, when applied together, have two dark states that are not affected by the interactions $|\uparrow\uparrow\rangle|0\rangle$ and $|S\rangle|0\rangle$. The remaining basis states of the qubits, $|\downarrow\downarrow\rangle$ and $|T\rangle \equiv \frac{1}{\sqrt{2}}(|\uparrow\downarrow\rangle + |\downarrow\uparrow\rangle)$, are driven by H_s and eventually pumped to $|\uparrow\uparrow\rangle|0\rangle$ by the combination of the sideband drive and the sympathetic cooling (Fig. 1b). The effect of adding the carrier drive H_c is to couple the $|\uparrow\uparrow\rangle$ state to a combination of the $|\uparrow a\rangle$, $|a\uparrow\rangle$ and $|aa\rangle$ states and the $|S\rangle$ state to the $|S_a\rangle \equiv \frac{1}{\sqrt{2}}(|a\downarrow\rangle - |\downarrow a\rangle)$ state. However, assuming the ions are in the ground state of motion, the dressed states of the sideband Hamiltonian H_s containing $|S_a\rangle$ have eigenenergies $\pm\Omega_s$, while $|S\rangle$, $|\uparrow\uparrow\rangle$, $|\uparrow a\rangle$ and $|a\uparrow\rangle$ are dark states of H_s with zero eigenenergy. Thus, the transition from $|S\rangle|0\rangle$ to $|S_a\rangle|0\rangle$ is shifted out of resonance with the carrier drive and therefore suppressed for $\Omega_c \ll \Omega_s$. On the other hand, the transitions from the $|\uparrow\uparrow\rangle|0\rangle$ state to the $|\uparrow a\rangle|0\rangle$ and $|a\uparrow\rangle|0\rangle$ states are not energy shifted and remain resonant. The repumping laser incoherently transfers the state $|a\rangle$ back to the $|\uparrow\rangle$ and $|\downarrow\rangle$ qubit manifold. Thus, the combination

[1]National Institute of Standards and Technology, 325 Broadway, Boulder, Colorado 80305, USA. [2]QUANTOP, The Niels Bohr Institute, University of Copenhagen, Blegdamsvej 17, DK-2100 Copenhagen Ø, Denmark.

*These authors contributed equally to this work.

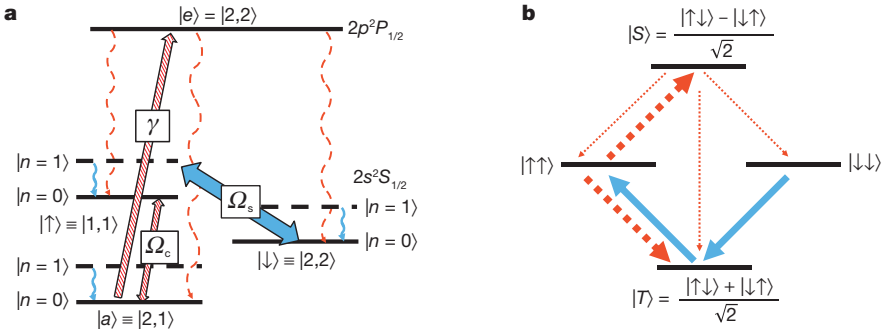

Figure 1 | Energy levels and entanglement preparation scheme. a, The internal energy levels (not to scale) of $^{9}Be^{+}$ are shown as thick solid black lines for the ground motional state and dashed lines for the first excited motional state. The couplings needed to produce steady-state entanglement are shown with blue arrows for the strong sideband coupling (Ω_s) and sympathetic cooling, and by patterned and dashed red arrows for the weak microwave coupling (Ω_c), repumping (γ), and spontaneous emission from the $|e\rangle$ state. Wavy arrows depict the dissipative processes. **b**, Four spin states that span the $|\uparrow\rangle$, $|\downarrow\rangle$ qubit manifold of the two $^{9}Be^{+}$ ions are shown as horizontal lines. Transfer processes that are accomplished by the sideband drive and sympathetic cooling are shown as blue arrows, whereas processes that occur by coupling the $|\uparrow\rangle$ state to the auxiliary $|a\rangle$ state followed by excitation with the repumping beam and decay by spontaneous emission are shown as dashed red arrows. Processes shown as thin dotted red lines are shifted out of resonance owing to the strong sideband coupling, leading to accumulation of population in the maximally entangled state $|S\rangle$ in steady state. Further details about the rates for each process are given in Supplementary Information.

of H_c and the repumping beam create a process to pump $|\uparrow\uparrow\rangle$ to $|S\rangle$ as well as a depumping process from $|S\rangle$ to $|\downarrow\downarrow\rangle$, $|T\rangle$ and $|\uparrow\uparrow\rangle$, although the latter is significantly slower (Fig. 1b). In the limit where the rate of pumping other states into $|S\rangle$ is much greater than the depumping rate from $|S\rangle$, the steady state will approach $|S\rangle$. The ratio of these rates can be made arbitrarily high by reducing the values of γ, κ and Ω_c compared to Ω_s and in steady state the fidelity of the maximally entangled state $|S\rangle$ can approach unity (see Supplementary Information). Fluctuations in the values of these parameters do not reduce the fidelity of the entangled state as long as the values of γ, κ and Ω_c remain small compared to Ω_s, which is in contrast to the method of entanglement preparation via unitary gates.

For our experimental implementation, we confine a $^{9}Be^{+}$–$^{24}Mg^{+}$–$^{24}Mg^{+}$–$^{9}Be^{+}$ four-ion chain in a linear radio-frequency Paul trap[10]. The two $^{9}Be^{+}$ ions serve as qubit ions while the two $^{24}Mg^{+}$ ions are used for sympathetic cooling. The ion chain lies along the axis of the trap, the axis of weakest confinement, and has an extent of approximately 11 μm. We label the four-ion axial modes {1, 2, 3, 4}, and they have mode frequencies $\nu_{1-4} \approx \{2.0, 4.1, 5.5, 5.8\ \mathrm{MHz}\}$, respectively. An internal-state quantization magnetic field $B \approx 11.964$ mT is applied along a direction that is at 45° to the trap axis, which breaks the degeneracy of the magnetic sub-levels of $^{9}Be^{+}$ and $^{24}Mg^{+}$. As depicted in Fig. 1a, we utilize the $^{9}Be^{+}$ internal states $|F = 1, m_F = 1\rangle \equiv |\uparrow\rangle$, $|2, 2\rangle \equiv |\downarrow\rangle$ and $|2, 1\rangle \equiv |a\rangle$. To create the sideband coupling term H_s, we apply two 313 nm laser beams in a Raman configuration tuned approximately 270 GHz below the $2s\ ^{2}S_{1/2}$ to $2p\ ^{2}P_{1/2}$ transition with a frequency difference equal to $f_0 + \nu_3$ where $f_0 \approx 1.018$ GHz is the resonant transition frequency between the $|\downarrow\rangle$ and $|\uparrow\rangle$ states. The two beams are derived from the same laser and frequency-shifted using acousto-optic modulators. The difference wave vector of the two beams is parallel to the trap axis. Microwaves are used to drive resonant transitions between the $|\uparrow\rangle$ state and the $|a\rangle$ state ($f \approx 1.121$ GHz) to create H_c. We also apply a repump laser beam to drive the $|a\rangle$ state to the $2p\ ^{2}P_{1/2}|2, 2\rangle$ state, which subsequently spontaneously emits a photon and decays to $|\uparrow\rangle$, $|\downarrow\rangle$ or $|a\rangle$ with a branching ratio of approximately 5:4:3. Phonon excitations due to the photon recoil are removed by the sympathetic cooling. To cool the $^{24}Mg^{+}$ ions, a Doppler cooling beam, two Raman-sideband beams, and a repump beam co-propagate with the $^{9}Be^{+}$ Raman beams. These beams ($\lambda \approx 280$ nm) interact negligibly with the internal states of the $^{9}Be^{+}$ ions. We initialize each experiment by first applying Doppler cooling to $^{9}Be^{+}$ and $^{24}Mg^{+}$, followed by $^{24}Mg^{+}$ sideband cooling of all the axial modes to near the ground state of motion. An optical pumping pulse initializes the $^{9}Be^{+}$ ions to the $|\downarrow\downarrow\rangle$ state. We then apply the dissipative entanglement preparation operations, as detailed below. Finally, we perform spin-state analysis to measure the populations of the $|S\rangle$, $|T\rangle$, $|\uparrow\uparrow\rangle$ and $|\downarrow\downarrow\rangle$ spin states (see Methods).

We implement the entanglement scheme using mode 3, where the $^{9}Be^{+}$ ions oscillate in phase with each other but out of phase with the $^{24}Mg^{+}$ ions (which oscillate in phase). In one implementation of the experiment, we apply the laser-induced sideband excitation, microwave-induced carrier excitation, repumping and sympathetic cooling simultaneously (see Methods for parameter values) for a duration t and obtain a steady-state singlet state fidelity of 0.75(3), as shown in Fig. 2.

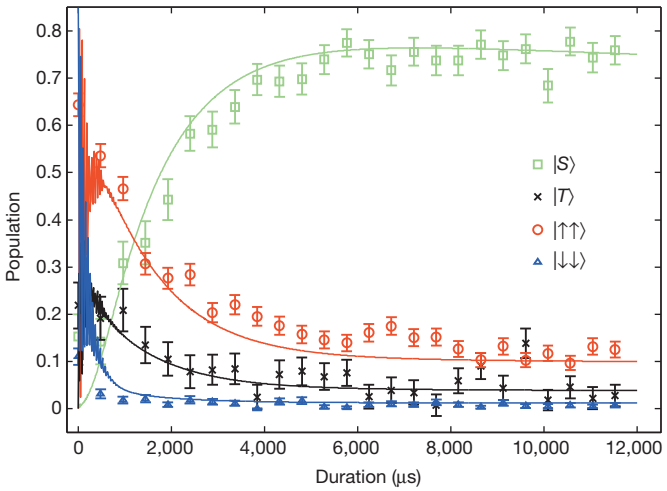

Figure 2 | Steady-state entanglement. Measured populations of the singlet, triplet, $|\uparrow\uparrow\rangle$ and $|\downarrow\downarrow\rangle$ states (respectively squares, crosses, circles and triangles) are shown as a function of duration; the duration is the length of time during which all elements of the dissipative entanglement scheme are applied simultaneously. The system reaches a steady state with a 0.75(3) population in the target singlet state after a few milliseconds. The solid lines are the result of a simulation based on the experimental parameters (see Methods). The slow decrease in the singlet state fidelity at long times visible in the simulation is due to a leak of the qubits to spin states outside the $|\uparrow\rangle$, $|\downarrow\rangle$, $|a\rangle$ manifold caused by spontaneous emission from the lasers that generate the sideband coupling (see Methods and Supplementary Information). Strictly speaking this depumping means that the state is only a quasi-steady state. For our parameters there is, however, a clear separation of the preparation and depumping timescales, justifying the description as a steady state. Data are shown as mean ± s.d.

We model the experiment (solid lines in Fig. 2) taking into account: (1) the additional spontaneous emission due to the off-resonant $^9Be^+$ sideband laser beams, (2) the position fluctuations of those beams at the ions' location, which leads to unequal sideband Rabi rates for the two $^9Be^+$ ions, (3) off-resonant coupling of the sideband excitation to other motional modes, and (4) heating processes (see Methods). The model is in close agreement with the data and suggests that the resulting state is an incoherent mixture of $|S\rangle$ and other states (mainly $|\uparrow\uparrow\rangle$) and the dominant errors come from the spontaneous emission induced by the sideband laser beams and unequal sideband Rabi rates.

We also implement the scheme in a stepwise manner. In this case, we can take advantage of coherences to speed up the entanglement creation process and thereby reduce the effect of the spontaneous emission induced by the $^9Be^+$ sideband laser beams. Specifically, we apply a sequence of steps, with each step consisting of a coherent pulse with $H_{coh} = H_s + H_c$ followed by the dissipative processes of repumping and sympathetic cooling, applied sequentially (the order does not matter). In the steady-state entanglement procedure outlined above, we required Ω_c, γ, $\kappa \ll \Omega_s$ to suppress transitions from $|S\rangle$ to $|S_a\rangle$. However, when H_{coh} is applied without any dissipation, ions initially in the $|S\rangle$ state will oscillate between $|S\rangle$ and a superposition of $|S\rangle$ and $|S_a\rangle$, which is dressed by H_s, with a period of $2\pi/\sqrt{\Omega_s^2+\Omega_c^2}$, assuming the ions are in the motional ground state. Thus, by applying H_{coh} for a full oscillation period the interaction will be an identity operation for the $|S\rangle$ state while all other states will be partially transferred to the auxiliary level $|a\rangle$, which can then be repumped to create $|S\rangle$. However, if $n \neq 0$ some population will be transferred out of the $|S\rangle$ state because the oscillation period is dependent on n. By taking advantage of the coherent evolution, we relax the requirement Ω_c, γ, $\kappa \ll \Omega_s$ and the entanglement preparation timescale can be shortened, which reduces the error due to spontaneous emission induced by the sideband laser beams. During the coherent process, the entangled state $|S\rangle$ is no longer strictly a steady state; however, if the ratio Ω_c/Ω_s is small, the evolution of the state away from $|S\rangle$ will be correspondingly small and $|S\rangle$ remains an approximate steady state.

The results of the stepwise experiment are shown in Fig. 3. We obtain the singlet state with fidelity 0.89(2). We use the same model as for the continuous case to predict the outcome of the stepwise scheme, and find good agreement with the data (solid lines in Fig. 3), with the largest sources of error coming from heating processes, unequal sideband Rabi rates, spontaneous emission caused by the $^9Be^+$ sideband lasers and off-resonant coupling of the sideband to mode 4.

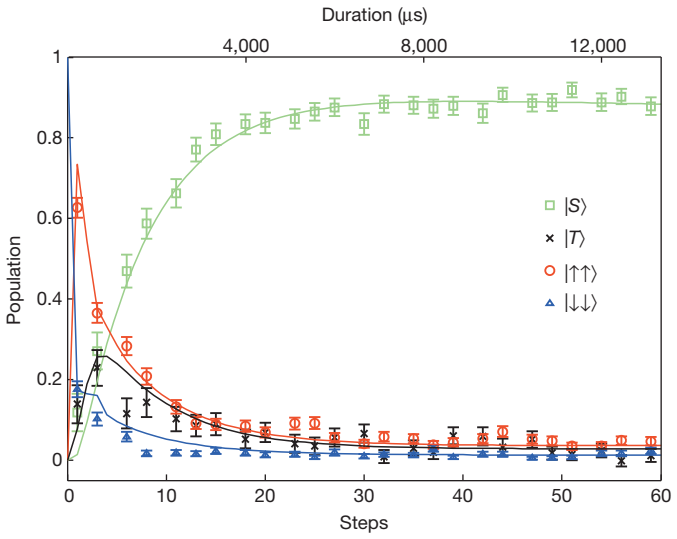

Figure 3 | Entanglement with stepwise scheme. The measured populations of the singlet, triplet, $|\uparrow\uparrow\rangle$ and $|\downarrow\downarrow\rangle$ states (respectively squares, crosses, circles and triangles) are shown as a function of the number of applied steps. Each step has a duration of approximately 220 μs. The solid lines are the results of a model (see Methods). Data are shown as mean ± s.d.

We have presented deterministic steady-state pumping into a maximally entangled state with fidelities that are limited by known experimental imperfections. This result can be extended to other systems where two-qubit quantum logic gates may not be feasible owing to strong dissipation[22], and represents a step towards harnessing dissipation for quantum information processing.

METHODS SUMMARY

The Methods section includes detailed descriptions of (1) the state detection and analysis procedure, (2) the experimental parameters for continuous and stepwise implementation of the scheme, and (3) the theoretical model used to produce the solid lines in Figs 2 and 3.

Online Content Any additional Methods, Extended Data display items and Source Data are available in the online version of the paper; references unique to these sections appear only in the online paper.

Received 18 July; accepted 16 October 2013.
Published online 24 November 2013.

1. Nielsen, M. A. & Chuang, I. L. *Quantum Computation and Quantum Information* (Cambridge Univ. Press, 2000).
2. Ladd, T. D. *et al.* Quantum computers. *Nature* **464,** 45–53 (2010).
3. Krauter, H. *et al.* Entanglement generated by dissipation and steady state entanglement of two macroscopic objects. *Phys. Rev. Lett.* **107,** 080503 (2011).
4. Barreiro, J. T. *et al.* An open-system quantum simulator with trapped ions. *Nature* **470,** 486–491 (2011).
5. Kraus, B. *et al.* Preparation of entangled states by quantum Markov processes. *Phys. Rev. A* **78,** 042307 (2008).
6. Diehl, S. *et al.* Quantum states and phases in driven open quantum systems with cold atoms. *Nature Phys.* **4,** 878–883 (2008).
7. Verstraete, F., Wolf, M. M. & Cirac, J. I. Quantum computation and quantum-state engineering driven by dissipation. *Nature Phys.* **5,** 633–636 (2009).
8. Shankar, S. *et al.* Autonomously stabilized entanglement between two superconducting quantum bits. *Nature* http://dx.doi.org/10.1038/nature12802 (this issue).
9. Lanyon, B. P. *et al.* Universal digital quantum simulation with trapped ions. *Science* **334,** 57–61 (2011).
10. Hanneke, D. *et al.* Realization of a programmable two-qubit quantum processor. *Nature Phys.* **6,** 13–16 (2010).
11. Sayrin, C. *et al.* Real-time quantum feedback prepares and stabilizes photon number states. *Nature* **477,** 73–77 (2011).
12. Vijay, R. *et al.* Stabilizing Rabi oscillations in a superconducting qubit using quantum feedback. *Nature* **490,** 77–80 (2012).
13. Ristè, D., Bultink, C. C., Lehnert, K. W. & DiCarlo, L. Feedback control of a solid-state qubit using high-fidelity projective measurement. *Phys. Rev. Lett.* **109,** 240502 (2012).
14. Brakhane, S. *et al.* Bayesian feedback control of a two-atom spin-state in an atom-cavity system. *Phys. Rev. Lett.* **109,** 173601 (2012).
15. Schindler, P. *et al.* Quantum simulation of dynamical maps with trapped ions. *Nature Phys.* **9,** 361–367 (2013).
16. Campagne-Ibarcq, P. *et al.* Persistent control of a superconducting qubit by stroboscopic measurement feedback. *Phys. Rev. X* **3,** 021008 (2013).
17. Ristè, D. *et al.* Deterministic entanglement of superconducting qubits by parity measurement and feedback. *Nature* **502,** 350–354 (2013).
18. Poyatos, J. F., Cirac, J. I. & Zoller, P. Quantum reservoir engineering with laser cooled trapped ions. *Phys. Rev. Lett.* **77,** 4728–4731 (1996).
19. Plenio, M. B., Huelga, S., Beige, A. & Knight, P. L. Cavity-loss-induced generation of entangled atoms. *Phys. Rev. A* **59,** 2468–2475 (1999).
20. Clark, S., Peng, A., Gu, M. & Parkins, S. Unconditional preparation of entanglement between atoms in cascaded optical cavities. *Phys. Rev. Lett.* **91,** 177901 (2003).
21. Parkins, A. S., Solano, E. & Cirac, J. I. Unconditional two-mode squeezing of separated atomic ensembles. *Phys. Rev. Lett.* **96,** 053602 (2006).
22. Kastoryano, M. J., Reiter, F. & Sørensen, A. S. Dissipative preparation of entanglement in optical cavities. *Phys. Rev. Lett.* **106,** 090502 (2011).
23. Cho, J., Bose, S. & Kim, M. S. Optical pumping into many-body entanglement. *Phys. Rev. Lett.* **106,** 020504 (2011).
24. Bermudez, A., Schaetz, T. & Plenio, M. B. Dissipation-assisted quantum information processing with trapped ions. *Phys. Rev. Lett.* **110,** 110502 (2013).
25. Leghtas, Z. *et al.* Stabilizing a Bell state of two superconducting qubits by dissipation engineering. *Phys. Rev. A* **88,** 023849 (2013).
26. Reiter, F., Tornberg, L., Johansson, G. & Sørensen, A. S. Steady state entanglement of two superconducting qubits by engineered dissipation. *Phys. Rev. A* **88,** 032317 (2013).
27. Cormick, C., Bermudez, A., Huelga, S. F. & Plenio, M. B. Dissipative ground-state preparation of a spin chain by a structured environment. *New J. Phys.* **15,** 073027 (2013).
28. Ticozzi, F. & Viola, L. Steady-state entanglement by engineered quasi-local Markovian dissipation: Hamiltonian-assisted and conditional stabilization.

Quantum Inform. Comput. (in the press); preprint at http://arXiv.org/abs/1304.4270 (2013).
29. Barrett, M. D. *et al.* Sympathetic cooling of $^{9}Be^{+}$ and $^{24}Mg^{+}$ for quantum logic. *Phys. Rev. A* **68,** 042302 (2003).
30. Reiter, F. & Sørensen, A. S. Effective operator formalism for open quantum systems. *Phys. Rev. A* **85,** 032111 (2012).

Supplementary Information is available in the online version of the paper.

Acknowledgements This research was funded in part by the Office of the Director of National Intelligence (ODNI), Intelligence Advanced Research Projects Activity (IARPA). All statements of fact, opinion or conclusions contained herein are those of the authors and should not be construed as representing the official views or policies of IARPA or the ODNI. This work was also supported by ONR, by the NIST Quantum Information Program, and by the European Union's Seventh Framework Program through SIQS (grant no. 600645) and through the ERC grant QIOS (grant no. 306576). We thank D. Allcock and B. Sawyer for comments on the manuscript and E. Knill for conversations. F.R. acknowledges conversations with B. Lanyon, R. Blatt and J. Home and support from the Studienstiftung des deutschen Volkes. This Letter is a contribution of NIST and is not subject to US copyright.

Author Contributions Y.L. and J.P.G. performed the experiments, analysed the data and developed the numerical model. F.R. proposed the entanglement scheme and developed the analytic rate model described in Supplementary Information under the guidance of A.S.S. T.R.T. contributed to the numerical model and the experimental apparatus. R.B. contributed to the experimental apparatus. D.L. and D.J.W. directed the experiments. All authors provided important suggestions for the experiments, discussed the results and contributed to the manuscript.

Author Information Reprints and permissions information is available at www.nature.com/reprints. The authors declare no competing financial interests. Readers are welcome to comment on the online version of the paper. Correspondence and requests for materials should be addressed to Y.L. (yiheng.lin@colorado.edu).

METHODS

Spin-state fidelity measurement. To detect the populations of the $|S\rangle$, $|T\rangle$, $|\uparrow\uparrow\rangle$ and $|\downarrow\downarrow\rangle$ states, we need to obtain the relevant elements of the density matrix ρ describing the state of the two $^9Be^+$ ions during the experiment. Because each ion may be found in any of the three ground states $|\uparrow\rangle$, $|\downarrow\rangle$, $|a\rangle$ (Fig. 1), the density matrix has dimensions 9×9. The singlet-state population is given by $\frac{1}{2}(\rho_{\uparrow\downarrow,\uparrow\downarrow}+\rho_{\downarrow\uparrow,\downarrow\uparrow})-\mathrm{Re}(\rho_{\uparrow\downarrow,\downarrow\uparrow})$ and the triplet-state population is given by $\frac{1}{2}(\rho_{\uparrow\downarrow,\uparrow\downarrow}+\rho_{\downarrow\uparrow,\downarrow\uparrow})+\mathrm{Re}(\rho_{\uparrow\downarrow,\downarrow\uparrow})$. The fidelity of the target entangled state, F, is equal to the singlet-state population. For the steady-state fidelity, we report the average fidelity measured between 6 and 12 ms for the continuous case and between 35 and 59 steps in the stepwise case. We first measure the populations of the $|\downarrow\rangle$ state by collecting fluorescence photons from the laser-induced cycling transition $|\downarrow\rangle\leftrightarrow 2p\,^2P_{3/2}|3,3\rangle$ of both $^9Be^+$ ions together. We apply this detection beam for 250 μs and collect photon counts with a photomultiplier tube (approximately 30 counts are registered per ion in the $|\downarrow\rangle$ state). We repeat the experiment and detection 400 times to obtain a histogram. We fit the histogram of counts to a Poisson distribution to obtain the probabilities to measure both ions, one ion and zero ions in the $|\downarrow\rangle$ state denoted by P_2, P_1 and P_0, respectively. Specifically, these probabilities are related to the density matrix as follows: $P_2=\rho_{\downarrow\downarrow,\downarrow\downarrow}$, $P_1=\rho_{\downarrow\uparrow,\downarrow\uparrow}+\rho_{\uparrow\downarrow,\uparrow\downarrow}+\rho_{a\downarrow,a\downarrow}+\rho_{\downarrow a,\downarrow a}$, and $P_0=\rho_{\uparrow\uparrow,\uparrow\uparrow}+\rho_{a\uparrow,a\uparrow}+\rho_{\uparrow a,\uparrow a}+\rho_{aa,aa}$. We repeat the entanglement preparation scheme and perform a microwave π pulse on the $|\downarrow\rangle\leftrightarrow|\uparrow\rangle$ transition followed by the same detection procedure to obtain: $P_{2,\pi}=\rho_{\uparrow\uparrow,\uparrow\uparrow}$, $P_{1,\pi}=\rho_{\uparrow\downarrow,\uparrow\downarrow}+\rho_{\downarrow\uparrow,\downarrow\uparrow}+\rho_{a\uparrow,a\uparrow}+\rho_{\uparrow a,\uparrow a}$, and $P_{0,\pi}=\rho_{\downarrow\downarrow,\downarrow\downarrow}+\rho_{a\downarrow,a\downarrow}+\rho_{\downarrow a,\downarrow a}+\rho_{aa,aa}$. Thus, assuming the population of the $|aa\rangle$ state is negligible (see below), we have $\rho_{\uparrow\downarrow,\uparrow\downarrow}+\rho_{\downarrow\uparrow,\downarrow\uparrow}=P_1-(P_{0,\pi}-P_2)$. To obtain the off-diagonal elements, we perform the same experiment but with a microwave π/2 pulse on the $|\downarrow\rangle\leftrightarrow|\uparrow\rangle$ transition before the detection to obtain $P_{2,\frac{\pi}{2}}$, $P_{1,\frac{\pi}{2}}$ and $P_{0,\frac{\pi}{2}}$. The phase of the microwave is randomized in each experiment. It can be shown that $\mathrm{Re}(\rho_{\uparrow\downarrow,\downarrow\uparrow})=-1/2+2P_{0,\frac{\pi}{2}}+\frac{1}{2}(P_2-P_0)+\frac{1}{2}(P_{2,\pi}-P_{0,\pi})$, which gives the last piece of information needed to obtain the populations of the $|S\rangle$ and $|T\rangle$ states.

Owing to spontaneous Raman scattering caused by the sideband laser beams, it is possible that the $^9Be^+$ ions could be transferred to a hyperfine state outside the $|\uparrow\rangle$, $|\downarrow\rangle$, $|a\rangle$ manifold. However, this detection procedure does not distinguish these states from the $|a\rangle$ state. Our model predicts that the probability to find at least one ion outside the three-state manifold is at most 5% for the data in Fig. 2 and 3% for the data in Fig. 3. In future experiments, this population could be brought back to the three-state manifold with additional repump beams.

To calculate the singlet fidelity above, we assumed that the probability to find both atoms outside the $|\uparrow\rangle$, $|\downarrow\rangle$ qubit manifold was negligible. For the data in Figs 2 and 3 we measured the probability to find at least one ion outside the qubit manifold state, given by $P_0+P_{0,\pi}-(P_2+P_{2,\pi})$, to be 7(5)% and 2(2)% respectively for the steady state. We expect the probability to find both ions outside the qubit manifold to be of the order of the square of the probability to find one ion outside the qubit manifold, which is therefore small. Furthermore, our theoretical model predicts the probability of finding both ions outside the qubit manifold to be at most 1% for the continuous implementation and 0.05% for the stepwise implementation.

Experimental parameters. For the continuous implementation of the scheme shown in Fig. 2, the sideband Rabi rate was $\Omega_s=2\pi\times 7.8(1)$ kHz and the microwave Rabi rate was $\Omega_c=2\pi\times 0.543(6)$ kHz. The 1/e time for the repump beam to deplete the $|a\rangle$ state was 88 μs. The 1/e time for continuous sympathetic sideband cooling of mode 3 was 203 μs; this was determined from an exponential fit of the average Fock-state occupation number $\bar{n}$ versus sympathetic cooling time from the initial Doppler-cooled value of $\bar{n}\approx 2.5$ to a steady-state value, with cooling on, of $\bar{n}=0.11(1)$. The continuous sympathetic cooling was achieved by applying the laser-induced Raman sideband for the $^{24}Mg^+$ ions that couples the electronic ground states $\left|F=\frac{1}{2},m_F=-\frac{1}{2}\right\rangle|n\rangle\leftrightarrow\left|\frac{1}{2},\frac{1}{2}\right\rangle|n-1\rangle$ simultaneously with a repump beam that transfers $\left|\frac{1}{2},\frac{1}{2}\right\rangle|n\rangle\rightarrow\left|\frac{1}{2},-\frac{1}{2}\right\rangle|n\rangle$. The continuous sympathetic cooling off-resonantly cooled the other axial modes 1, 2 and 4 with 1/e times of approximately 1,300 μs, 294 μs and 181 μs to thermal states with average Fock state occupation numbers of approximately 2.9, 0.95 and 0.12, respectively. The Rabi rate for the $^{24}Mg^+$ sideband transition on mode 3 was $\sim 2\pi\times 11.9$ kHz and the repumping rate was $\sim 2\pi\times 625$ kHz (corresponding to a 1/e repump time of 1.6 μs). The repumping rate was made significantly stronger than the sideband rate to eliminate any coherent dynamics between the $^{24}Mg^+$ spins and ion-crystal motion.

We implemented the stepwise scheme in the following way: in each step we first sympathetically cooled each of the modes of the $^9Be^+$–$^{24}Mg^+$–$^{24}Mg^+$–$^9Be^+$ chain with $^{24}Mg^+$ Raman sideband cooling[31,32], followed by application of H_{coh} for a duration $t_{2\pi}$, and at the end of each step we applied the repumping beam. The populations of the qubit state were measured at the end of each step and plotted in Fig. 3. The $^9Be^+$ sideband Rabi rate was $\Omega_s=2\pi\times 8.4(1)$ kHz and the microwave Rabi rate was $\Omega_c=2\pi\times 1.24(6)$ kHz. The repumping beam had a 1/e time of approximately 3 μs and was turned on for 6 μs in each step. In each step, two sympathetic cooling cycles were applied to mode 1, which has the largest heating rate, and one cycle was applied to each of the remaining modes, with mode 3 being the last. A sympathetic cooling cycle consists of a single motion subtracting sideband pulse applied to the $^{24}Mg^+$ ions followed by a repump pulse. The five cooling cycles were applied for a total duration of ~100 μs in each step.

In both cases, the ion spacing was set by adjusting the strength of the harmonic confinement, such that $\Delta_k z=2\pi m$ where $\Delta_k\approx\frac{2\pi\sqrt{2}}{313\times 10^{-9}}\ m^{-1}$ is the wavevector difference of the $^9Be^+$ Raman sideband lasers, z is the distance between the $^9Be^+$ ions, and m is an integer, such that the phase of the sideband excitation was equal on both ions. For our confinement strength, $z\approx 11$ μm such that the value of m was near 300. For modes where the qubit ions move in phase, the integer value of m ensures H_s is as defined in the main text. However, in the general case $H_s\equiv\Omega_s(|\uparrow\rangle_1\langle\downarrow|+e^{i\phi}|\uparrow\rangle_2\langle\downarrow|)b^+ + \mathrm{h.c.}$, where ϕ is the phase difference between the two $^9Be^+$ ions of the sideband coupling, and the steady state of the system (including the cooling, repumping and microwave carrier) is $|D_\phi\rangle\equiv\frac{|\uparrow\downarrow\rangle-e^{i\phi}|\downarrow\uparrow\rangle}{\sqrt{2}}$.

Numerical model. We modelled our experiment using a master equation with a coherent component describing the $^9Be^+$ sideband and microwave carrier drives and Lindblad operators describing the sympathetic cooling, repumping and spontaneous emission due to the $^9Be^+$ sideband lasers. The coherent Hamiltonian is

$$H_{coh}\equiv\Omega_s\left[\left(1-\frac{r}{2}\right)|\uparrow\rangle_1\langle\downarrow|+\left(1+\frac{r}{2}\right)|\uparrow\rangle_2\langle\downarrow|\right)b^+ + \Omega_c\left(|a\rangle_1\langle\uparrow|+|a\rangle_2\langle\uparrow|\right)+\mathrm{h.c.}$$

where r describes the Rabi-rate imbalance of the sideband on the two ions. The Lindblad operator describing sympathetic cooling is given by $L_\kappa=\sqrt{\kappa}b$, and the repumping is given by $L_{\gamma_{j,a}}$, where j is either the $|\uparrow\rangle$ or $|\downarrow\rangle$ state and $L_{\gamma_{j,a}}=\sqrt{\gamma_{j,a}}|a\rangle$. Heating processes that limit the sympathetic cooling are modelled with a Lindblad operator $L_{\kappa_h}=\sqrt{\kappa_h}b^\dagger$, where κ_h is determined experimentally by measuring $\bar{n}$ for mode 3 after sympathetic cooling (no other interactions are turned on). The heating rate is given by $\kappa_h=\frac{\kappa\bar{n}}{1+\bar{n}}$. For the continuous cooling used for the data in Fig. 2 we found $\bar{n}=0.11(1)$ and for the stepwise case of Fig. 3 we found $\bar{n}=0.08(1)$. We take into account spontaneous emission that incoherently changes population from the state i to the state j ($i\neq j$) caused by the $^9Be^+$ sideband laser beams with Lindblad operators of the form $L_{j,i}=\sqrt{\Gamma_{j,i}}|j\rangle\langle i|$, where $\Gamma_{j,i}$ can be calculated using the Kramers-Heisenberg formula[33]. The error caused by Rayleigh scattering ($i=j$) is negligible[34]. Off-resonant coupling to mode 4 is taken into account with an additional Hamiltonian term $H_4=\Omega_s\frac{\eta_4}{\eta_3}\left(|\uparrow\rangle_1\langle\downarrow|-|\uparrow\rangle_2\langle\downarrow|\right)c^+e^{-i\delta t}+\mathrm{h.c.}$, where c^+ is the raising operator for the fourth mode, $\delta\approx 2\pi\times 250$ kHz is the splitting between modes 3 and 4, and $\eta_3=0.180$ and $\eta_4=0.155$ are the Lamb-Dicke parameters of modes 3 and 4, respectively. The continuous implementation of the scheme is modelled by numerically solving a master equation that includes all terms for a variable duration and a given value of r. We then obtain the theoretical prediction shown in Fig. 2 by averaging simulations with different values of r using a Gaussian distribution with an r.m.s. value of 0.014. This r.m.s. value was determined from fits to qubit Rabi flopping curves for a single $^9Be^+$ ion and for the $^9Be^+$–$^{24}Mg^+$–$^{24}Mg^+$–$^9Be^+$ ion chain. Percent-level fluctuations of Ω_s cause negligible changes to the predicted fidelity. The result of the calculation at the end of each step is plotted in Fig. 3. In both cases, the initial state of the $^9Be^+$ ions was taken to be $|\downarrow\downarrow\rangle|n=0\rangle$. The particular initial state chosen affects the dynamics only at short times and does not affect the steady state. All numerical models were implemented by use of the quantum optics toolbox[35].

31. Monroe, C. *et al.* Resolved-sideband Raman cooling of a bound atom to the 3D zero-point energy. *Phys. Rev. Lett.* **75,** 4011–4014 (1995).

32. Jost, J. D. *et al.* Entangled mechanical oscillators. *Nature* **459,** 683–685 (2009).
33. Ozeri, R. *et al.* Errors in trapped-ion quantum gates due to spontaneous photon scattering. *Phys. Rev. A* **75,** 042329 (2007).
34. Uys, H. *et al.* Decoherence due to elastic Rayleigh scattering. *Phys. Rev. Lett.* **105,** 200401 (2010).
35. Tan, S. M. A computation toolbox for quantum and atomic optics. *J. Opt. B* **1,** 424–432 (1999).